Role of nitrate in the production of iron-modified hydrochar for arsenic removal

Yiwei Zhang
Nanjing Normal University
Dandan Chen (dandanchen@njnu.edu.cn)
Nanjing Normal University https://orcid.org/0000-0002-5936-6176
Yutong Xing
Nanjing Normal University
Bangwei Liu
Nanjing Normal University
Yan Zhou
Nanjing Normal University
Ping Lu
Nanjing Normal University

Research Article

Keywords: Hydrochar, Iron modification, Ferric nitrate, Iron retentions, Arsenic, Mechanism

Posted Date: May 16th, 2023

DOI: https://doi.org/10.21203/rs.3.rs-2783365/v1

Abstract

Iron-modified biochar is a promising As adsorption material. Compared to biochar, hydrochar has better As adsorption characteristics due to its abundant functional group. Many studies on iron modification of biochars have been reported. However, there are no reports focusing on the iron modification of hydrochars with different iron species. In this paper, a novel As adsorption material, iron-modified hydrochar, was synthesized through one-step hydrothermal carbonization (HTC) of poplar sawdust by different iron species, i.e., $FeCl_3 \cdot 6H_2O$ (FC), $FeSO_4 \cdot 7H_2O$ (FS) and $Fe(NO_3)_3 \cdot 9H_2O$ (FN). The physicochemical properties, Fe binding stability, and As adsorption properties of hydrochars were examined to see how preparation conditions and iron species affected them. Results showed that the iron retention rate and As adsorption capacity of hydrochar modified by FN were much higher than those modified by FS and FC. Moreover, these two increased proportionally with the increasing iron dosage. However, preparation time had limited effect on them. In addition, the functioning of FN in HTC was investigated to determine the key to enhancing the iron content of hydrochars in HTC. The As adsorption mechanism of iron-modified hydrochars was also studied to analyze the key to improve its As adsorption capacity. This paper will provide useful information for improving the preparation of iron-modified hydrochars and its As adsorption capacity.

Highlights

·Hydrochar with stable iron load was successfully synthesized by one step HTC method

·Effects of iron species on iron stability and As adsorption capacity was studied

·The As adsorption capacity of 8%FN@HC was the highest, reaching 11.19 mg/g

·•OH radical was a key factor affecting the iron loading of hydrochars

1. Introduction

The arsenic pollution of water and soil represents a pervasive and significant environmental problem(da Silva et al., 2019). The arsenic pollution has affected more than 100 million people and its main cause was natural geological sources (Bibi et al., 2017). Arsenic primarily occurs in contaminated water and sediment as arsenite (As(III)) and arsenate (As(V)). The International Agency for Research on Cancer classifies inorganic arsenic compounds as the group I human carcinogens, with As(III) being more hazardous than As(V)(Medunić et al., 2020). The World Health Organization has established a recommended limit of 10 μg/L for arsenic in potable water; however, arsenic levels in many regions have exceeded this limit, resulting in severe health effects(Hao et al., 2018).

Biochar, a carbon-rich solid material, has been identified as a prospective adsorbent material due to its exceptional adsorption efficacy on a variety of environmental pollutants. Consequently, numerous researchers have devoted their attention to this area(Lyu et al., 2020; Rashid et al., 2021; Wang, H. et al., 2021). It is frequently characterized by a wealth of functional groups and active sites, making it a promising adsorbent material. In nature water, arsenic primarily exists as arsenate and arsenite. However,

most unmodified biochar is negatively charged. Ali et al. studied As(V) adsorption characteristic by an almond shell biochar prepared at 450°Cand its maximum arsenic adsorption capacity (q_m) was 3.6mg/g(Ali et al., 2020). Due to the lack of electrostatic repulsion, the As adsorption efficiency of unmodified biochar is typically low(Li et al., 2019).

In several research, it has been demonstrated that the surface charge of biochar could be altered by modifying it with metal oxides, resulting in an increased capacity for anion adsorption(Chin et al., 2022; Gong et al., 2022; Liu, M. et al., 2021). Among metal oxides, iron oxides were identified as particularly effective adsorbents for arsenic(Abdelrhman et al., 2022; Sorlini et al., 2014). Under certain conditions, the functional group of iron oxide could be transferred onto the biochar surface, resulting in a modification in its surface charge and increased arsenate adsorption capacity(Vieira et al., 2017; Zoroufchi Benis et al., 2020). According to Cha et al., the maximum As(V) adsorption capacity of biochar modified with FeO_x at 800°C was improved to 6.8mg/g(Cha et al., 2021). By co-precipitating $Fe(NO_3)_3$ with KOH, Zhu et al. produced several nanosized goethite-modified biochars. The maximal adsorption capacity of modified biochar for As(III) was reported to be 62.79 times that of the initial(Zhu et al., 2020). However, biochar produced by pyrolysis requires relatively high reaction temperatures and its modification requires many steps, which greatly increase the cost and energy consumption of the preparation process.

According to previous research, hydrothermal carbonization (HTC) is a type of thermochemical conversion technology that directly synthesizes solid carbon in a liquid medium at moderate temperature and autogenic pressure(Li et al., 2022; Liang et al., 2021). Compared with pyrolytic biochar, hydrochar contains abundant carboxyl, hydroxyl, and other functional groups in the preparation process, which is the main advantages of metal adsorption. Functional groups could stabilize metal complexes while promoting electrostatic attraction. The low surface area and sparse, porous structure of hydrochar limit its application efficiency. Therefore, it needed to increase the hydrochars' porosity and adsorption sites in order to increase their heavy metal adsorption capacity(Chen et al., 2022; Luo et al., 2020). Iron modification was a promising method to enhance the porosity and adsorption sites. According to Capobianco et al., the As(V) removal characteristic was investigated by using $FeCl_3$-modified olive residue hydrochar prepared at 180°C(Capobianco et al., 2020). The results demonstrated that iron deposition on hydrochar was facilitated by the HTC process and that its As(V) adsorption capacity was higher (4.1 mg/g). However, the As adsorption capacity was still limited. Thus, it is necessary to analyze the mechanism of iron modification in HTC. However, few studies had been reported in this field. According to several studies, the adsorption capacity of hydrochar for heavy metals largely depends on production conditions and source materials (Fang et al., 2018; Liu, Z. et al., 2021). According to Zhang et al., temperature was the key factor in initiating ionic reactions in the subcritical region in HTC process(Zhang et al., 2021). The temperature increase during the HTC process can impact the viscosity of water, thus making it easier to penetrate the porous medium, thus further degrading the biomass and improving the pore structure of biomass(Khan et al., 2019). Therefore, in this research, the role of iron species and preparation conditions in the HTC process was explored to reveal the influence mechanism of different ions and operating conditions on the properties of iron-modified hydrochar and thus to improve the As adsorption performance of iron-modified hydrochar.

This paper aims to propose a novel As adsorbent carbon material through one-step hydrothermal carbonization, i.e., iron-modified hydrochar. In this paper, the synthesis method of iron-modified hydrochars was optimized based on its physicochemical and As adsorption characteristic when modified by different iron species. The iron retention rate of iron-modified hydrochars was measured in this paper to evaluate its iron loading characteristics and iron binding stability. Moreover, the As adsorption mechanisms were studied to analyze the key role of iron-modified hydrochars in As adsorption. In addition, the function of the iron species during the HTC process was investigated to determine why the iron loading yield of hydrochars improved when modified by specific iron species. These results will provide crucial information for the production of inexpensive and extremely effective As-adsorbing iron-modified hydrochars.

2. Materials and methods

2.1. Raw biomass and chemicals

Poplar wood sawdust (PW)was obtained from a sawmill in Lianyungang City, Jiangsu Province, China. The PW was desiccated in the oven at 105°C while a constant weight was achieved and was then ground mechanically in a pulverizer. Finally, the dried and ground PW was sieved to less than 2 mm particle size. $FeCl_3 \cdot 6H_2O$ (≥ 99.0%) (FC), $FeSO_4 \cdot 7H_2O$ (≥ 99.0%) (FS) and $Fe(NO_3)_3 \cdot 9H_2O$ (≥ 99.0%) (FN) used in this experiment were purchased from China Sinopharm Group.

2.2. Experiment

2.2.1 Preparation of iron-modified hydrochar

Iron-modified PW hydrochar (PWC) was synthesized via a one-step hydrothermal carbonization (HTC) process, whereby 25g of PW biomass was mixed with 250mL of a 10%w/v iron solution in a 500mL multifunctional reactor (MC500, Beijing Century Senlong, China). Table S1. demonstrates the preparation conditions. Before the HTC treatment, a nitrogen atmosphere was created in the reaction vessel by introducing 2 L/min of nitrogen over the course of 10 minutes. The rate of heating was set to 3°C/min, the initial pressure was maintained at 1 MPa, and the agitation rate was set to 100 r/min. The temperature (T) of the HTC reaction was set to 220°C, and the preparation time (τ) at this temperature varied within 60–480 minutes. Upon completion of the reaction, the reaction vessel was swiftly removed from the heating source and attained ambient temperature by immersion in cold water. The solid matter (hydrochar) was then filtered through filter paper with a 20 μm pore size, rinsed, and desiccated at 105°C until a constant weight was attained.

Hydrochar produced under different reaction conditions was named as X%FY@HC-ZZ. Among them, X represents iron dosage, i.e., the mass ratio of iron in the feed iron solution to the added PW during HTC. FY denotes the iron species, HC represents hydrochar, and ZZ is the preparation time. If not marked, the default preparation time is 120 min. For example, 6%FN@HC-480 represents the hydrochar obtained by using 0.107mol/L $Fe(NO_3)_3$ solution (6% iron dosage) at 220°C for 480 min. The HTC experiments were repeated

twice under varying conditions to confirm reproducibility and consistency. The average values obtained from the experimental repetitions were utilized for the subsequent analysis and discussion.

2.2.2 Evaluation of iron binding stability

After preparation, the filtered hydrochar was suspended in 500 mL deionized water for the first wash, then repeatedly filtered with filter paper and dried (105°C, 24 h) to obtain dry hydrochar. The second wash were performed by suspending 240 mg of hydrochar ((after dehydrating at 105°C and pulverizing) in 100 mL of distilled water(Capobianco et al., 2020). The suspension was magnetically agitated for one hour before being filtered through paper with a 20 μm pore size. Iron loading and stability in hydrochar were determined by comparing initial solution iron concentrations, solution recovered after initial filtration, and solution recovered after first and second washing, respectively. The iron retention rate of iron-modified hydrochar after filtration (w_1), first wash (w_2) and second wash (w_3) were determined as follows:

$$w_1 = \frac{[Fe]_0 V_0 - [Fe]_f V_f}{[Fe]_0 V_0} 100$$

1

$$w_2 = \frac{[Fe]_0 V_0 - [Fe]_f V_f - [Fe]_1 V_1}{[Fe]_0 V_0} 100$$

2

$$w_3 = \frac{[Fe]_0 V_0 - [Fe]_f V_f - [Fe]_1 V_1 - [Fe]_2 V_2}{[Fe]_0 V_0} 100$$

3

The formula denoted iron concentration and solution volume by $[Fe]_i$ and V_i, respectively. The subscripts 0, f, 1 and 2 represent the initial solution, the solution recovered after initial filtration, and the solutions recovered following the first and second rinsing processes, respectively.

2.2.3 Characterization

Based on GB/T 28,731–2012, an approximative analysis was conducted to ascertain the ash content (A) of PW and hydrochar. Using an elemental analyzer, the samples' C, H, N, and S levels were determined. (Vario EL III, Elementar, Germany). To analyze the functional groups, present in the hydrochar, Fourier transform infrared (FTIR) absorption spectrum was obtained utilizing an infrared spectrometer (Frontier, Perkin Elmer, USA) in the 4000 − 400 cm range. An X-ray photoelectron spectrometer (XPS, ESCALAB 250Xi, ThermoFisher, USA) was used to examine the surface composition of the hydrochars. The C1s peak of 284.8 eV was used as a binding energy calibration reference. Using a specific surface area analyzer (NOVA 2200e, Quantachrome, USA), the specific surface area and pore structure of hydrochar under various conditions were analyzed. An inductively coupled plasma optical emission spectrometer (ICP-OES;

PLASMA3000, NCS, CHINA) was used to analyze the iron and arsenic values, and the axial observation method was used for the test. By means of scanning electron microscopy and energy dispersive spectroscopy (SEM-EDS, JSM-7401F, JEOL, Japan), the surface morphology and elemental distribution of hydrochar were analyzed.

2.2.4 Arsenic adsorption experiments

In 50 ml polypropylene centrifuge containers, preliminary adsorption tests for arsenic were conducted. In order to calculate the arsenic adsorption effectiveness, 40 mg of dried hydrochar was suspended in 20 mL of a 20 mg/L arsenic solution (As(III)/As(V)) using 0.01 M NaNO3 as a background electrolyte and shaken at 200 rpm for 1440 minutes. For each experiment, three replications were conducted, and the final arsenic adsorption efficiency was calculated using the mean value. In this investigation, all hydrochars generated under all conditions were evaluated.

In 20 mg/L As(III) and 40 mg/L As(V) solutions, kinetic experiments were conducted, respectively. At various intervals, including 10, 30, 60, 120, 240, 480, 600, 1200, and 1440 minutes, samples were collected. Using pseudo first-order and pseudo second-order kinetic models, the rate of arsenic adsorption was described.

Initial As(III) concentrations varied between 0.5 and 20 mg/L and initial As(V) concentrations varied between 5 and 40 mg/ L, respectively, in adsorption isotherm experiments. Hydrochar was added to the solution and shaken under the optimal conditions determined by kinetic tests. Both the Langmuir and the Freundlich models were used to analyze the isotherm data.

3. Results and discussion

3.1. Mass yield and Van Krevelen analysis

As shown in Fig. 1, the mass yield and ash composition of hydrochars were studied to determine the impact of iron species, iron dosage, and preparation time.(a). Figure 1(a) demonstrates that the mass yield of hydrochars dropped after iron solution addition and showed substantial variation across iron species, indicating that the iron solution promoted the hydrolysis of PW in hydrothermal process to varying degrees. During the HTC process, dehydration, decarboxylation, and polymerization usually happened, and some of the organic matter moved to the water phase, which decreased mass output(Fang et al., 2018; Jain et al., 2016). When iron solution was added, it can further destroy the extracellular polymer to form a relatively low molecular weight compound. Polysaccharides were typically decomposed during this process, making products of carboxylic acid and hydroxyl that were then dehydrated and decarboxylated, releasing H_2O and CO_2 and ultimately causing a decrease in yield(Ma et al., 2021). Moreover, compared with FC and FS solution modification, the mass yield reduction of hydrochar modified by FN was relatively small and its ash content relatively high. The ash content increased with the increasing of FN dosage. FN modification effectively changed the composition of hydrochar. The rise in ash content showed that FN-modified hydrochar could load more iron onto its surface. However, when the iron dosage exceeds a certain amount,

the mass yield of hydrochars decreased slightly. The main reason should be that the decrease of feedwater pH promoted the dehydration and decarboxylation in HTC process. Preparation time was also a critical element influencing the mass yield of hydrochar in the HTC process, as shown in Fig. 1(a), but it has less effect on ash content. This indicated that the iron loading was completed in a relatively short time. Instead, excessive residence time may cause the decomposition of hydrochar.

The normalized element composition and yield of the hydrochars were studied to determine the impact of iron species, iron dosage, and preparation time, and the findings were depicted in Fig. 1(b). Hydrochar's normalized elemental composition was calculated by dividing the total mass of carbon, hydrogen, and oxygen found in the hydrochar by the mass of the corresponding biomass used to create the hydrochar (on a dry basis)(Falco et al., 2011). After adding iron solutions, C, H, and O in the hydrochars decreased. It can be inferred that iron solutions can promote the dehydration and decarboxylation process in HTC process, thereby reducing the element's content. Compared with FC and FS, the oxygen content of hydrochar modified by FN was higher, indicating that NO_3^- promotes the loading of Fe and O. However, the carbon yield efficiency of hydrochars decreased with the increasing the FN concentration and preparation time. On the physicochemical properties of iron-modified hydrochar, the preparation conditions have a substantial effect.

In Fig. 1(c). is depicted the van Krevelen diagram of hydrochars. The H/C and O/C atomic ratios were a crucial criterion for discussing the aromatics content and degree of deoxygenation in the HTC process of PW(Volpe and Fiori, 2017). Compared to unmodified hydrochar, the H/C and O/C ratios of FC-modified hydrochar were lower, presumably because its acidity promoted the carbonization of the hydrochar. However, the hydrochars modified by using FS and FN produced opposite changes, indicating that these iron-modified hydrochars contains more oxygen-containing functional groups(Ma et al., 2021). For FN-modified hydrochar, the O/C ratio increased significantly, and this increase was correlated to the FN concentration, indicating that the oxygen-containing functional groups has a significant positive correlation with FN concentration. On the contrary, the O/C and H/C ratios of hydrochars decreased substantially as preparation time increased, indicating that prolonging preparation time can promote decarboxylation and dehydration during HTC. Therefore, it can be concluded that the iron species have significantly different effects on the hydrochars. Using a high concentration FN solution can effectively load iron onto the hydrochars and increase its oxygen-containing functional groups. Long preparation times, however, will result in excessive carbonization of the hydrochars, resulting in a decrease in mass yield and the loss of oxygen-containing functional groups, which may impact the arsenic adsorption capacity.

3.2. Characterization

Figure S1(a). displays the FTIR spectra of PWC and iron-modified PWC. The peaks near the bands at 3400 cm^{-1} and 1053 cm^{-1} on the spectrum were O–H stretching vibration and –OH bending vibration peaks. The peak at 2933 cm^{-1} was the stretching vibration of the aliphatic $–CH_2$ group, which was asymmetric. The absorption peaks at 1611 cm^{-1} and 1360 cm^{-1} were the stretching vibration peaks of aromatic rings C = C, C = O and C = O in carboxyl groups(Oliveira et al., 2014). The strong band at approximately 1440 cm^-

^{1} represents the CO or COO– vibration of single-bond carboxyl groups and lactones(Dong and Wang, 2016). The peak band at 1104 cm^{-1} reflects the C–O stretching vibration in the hydroxyl group, and the bands at 1030 cm^{-1} and 1053 cm^{-1} represent the stretching vibration of C–O–C and O–H. The peaks appear at 565 cm^{-1} were characteristic peaks of the stretching vibration of Fe–O(Wan et al., 2020; Wang, L. et al., 2021). Compared with PWC, the –OH vibration of hydrochars modified by FN was strengthened, and the corresponding Fe–O stretching vibration peak was generated. On hydrochars, FN can facilitate the loading of Fe and the production of –OH. According to studies, Fe–O is a functional group that readily forms complexes with metal ions and enhances the adsorption capacity of heavy metal particles(Liang et al., 2017). Moreover, Figure S1(b), (c) illustrates the effect of preparation time and iron concentration on the FTIR spectrum of iron-modified hydrochars. As depicted in Figure S1(b), as the iron dosage increased, the vibration of –OH and Fe–O became stronger, while the vibration of COO– became weaker, similarly to the van Krevelen plot. Based on Figure S1(a), it can observe that with the prolongation of preparation time, the carbonization degree of hydrochar was higher and the vibration of the characteristic peaks of functional groups including Fe–O and –OH was weakened. The preparation time had a significant impact on the hydrochar's properties.

Figure S2 depicts the wide scanning XPS spectra of hydrochars modified by various iron species, as well as their C 1s, O 1s, Fe 2p, and N 1s spectra. In contrast to 6%FC@HC and 6%FS@HC, a prominent iron peak could be seen on the surface of 6%FN@HC, as shown in Figure S2(a). The results demonstrated that iron oxide was effectively loaded onto the hydrochar surface. As shown in Fig.S2(c), (f), and (h), a peak at 530.7 eV can be observed in O 1s spectrum and was attributed to the Fe–O structure. The content of Fe–O in hydrochar modified by FN was obviously higher than those modified FS and FC, indicating more iron was loaded on the surface of hydrochar. Based on Fig.S2 (d), a satellite peak at 716.4 eV can be observed, which was attributed to α-Fe_2O_3. The α-Fe_2O_3 on hydrochar with a FN-modified surface was the major component in As adsorption(Priyadarshni et al., 2020).

The SEM diagrams of the original hydrochar and the hydrochars modified by different iron species were shown in Fig. 2. Cracks and carbon microspheres of different sizes were formed on the surface of the hydrochars after two hours of carbonization. García-Bordejé E et al. believed that cellulose first formed tiny carbon microspheres during carbonization, and then the tiny carbon microspheres would expand into relatively large carbon microspheres(Gonzalez-Dominguez et al., 2021). Spherical iron (~20 nm) nanoparticles aggregation can be clearly observed in the SEM image of 6%FN@HC. According to EDS analysis, carbon and oxygen comprise the bulk of hydrochars' outermost layers. According to SEM mapping, the presence of Fe on the surface of 6%FN@HC strongly correlates with the presence of O. However, unlike hydrochars modified by FN, no significant iron loading was observed for the hydrochars modified by FC and FS.

The specific surface and area pore structure of hydrochars were listed in Fig. S3 and Table S2. In contrast to PWC, the BET surface area of 6%FN@HC was approximately seven times that of PWC. Compared with hydrochars modified by FS and FC, the pore structure hydrochar modified by FN was better. The pore volume of 6%FN@HC was 3.6 and 10.4 times that of 6%FS@HC and 6%FC@HC, respectively. Moreover, the

pore structure of hydrochar were improved with the increasing iron dosage and preparation time. The preparation time had a greater effect on the pore structure of hydrochars. Moreover, the iron loading roughened the surface of hydrochars, which was also conducive to the formation of pores(Liang et al., 2017). Based on Fig. S3, PWC and iron-modified hydrochars were all mesoporous materials, and the curve models belonged to IUPAC Class IV.(a)(Cychosz and Thommes, 2018; Thommes et al., 2015). The adsorption behavior in mesoporous pores was determined by interaction and intermolecular forces. It can be inferred from Fig. S3 (a) (c) (e) that the initial single multilayer adsorption of modified hydrochar on the mesoporous wall was followed by pore condensation. The pore structure of hydrochars were significantly affected by the modification of different iron species and different preparation time. According to Fig. S3. (f), it can be observed that the formation of mesopores depended largely on the preparation time.

3.3. Fe binding stability

To evaluate the Fe binding stability of hydrochars, the Fe retention rate was calculated based on Section 2.2.2 and the results are depicted in Fig. 3. Based on Fig. 3(a), about 85.4% of Fe were retained in 6%FN@HC after the first filtration and the iron retention rate was only slightly decreased after the following two washes. However, only 26.3% and 23.7% of Fe were retained in 6%FS@HC and 6%FC@HC after the first filtration and the value decreased to 8.9% and 5% after two washes. Therefore, compared to FN, the Fe binding stability of hydrochars modified by FS and FC were not good. Interestingly, Capobianco et al. supported the vast majority of Fe on the hydrochar surface using $FeCl_3$ and NaOH at a reaction temperature of 180°C(Capobianco et al., 2020). This can be attributed to iron's tendency to produce oxides under alkaline conditions. In this study, a large amount of iron can be loaded on the surface of hydrochar by FN without adding additional alkaline solvent.

The effects of iron dosage and preparation time on Fe binding stability of hydrochars were shown in Fig. 3(b) and 5(c), respectively. The Fe retention rate and Fe binding stability increased with increasing Fe dosage, as shown in Fig. 3(b). The Fe retention rate did not increase as the Fe dosage exceeded 6%. However, as Fe dosage increased, the iron content of hydrochars increased. From Fig. 3(c), it could be deduced that preparation time had less effect on Fe retention rate and Fe binding stability. When preparation time exceeded 240 min, the Fe retention rate decreased, indicating that Fe loading occurred over a relatively short time in the HTC process and too long preparation time will lead to the decrease of Fe retention rate.

3.4. As adsorption characteristics and kinetic analysis

The adsorption characteristics of arsenic in iron-modified hydrochars were investigated based on the As adsorption experiment, and the outcomes were presented in Fig. 4. Compared with hydrochars modified by FS and FC, the As adsorption capacity of hydrochars modified by FN was obviously higher and it increased proportionally with the increasing Fe dosage. 8%FN@HC showed the highest As adsorption capacity (3.24 ± 0.02 mg/g for As(III) and 4.62 ± 0.19 mg/g for As (V)). Iron can form bidentate compounds with AsO_2^- and AsO_4^{3-}, respectively, and has an excellent capacity for adsorption for As (III) and As (V) (Priyadarshni

et al., 2020; Zhang et al., 2016). In combination with the analysis of the Fe retention rate in Section 3.3, the As adsorption capacity of iron-modified hydrochars was found to be closely related to its iron retention rate. It can be inferred that complexation was the primary reaction for arsenic adsorption of the iron-modified hydrochar. Moreover, based on the pore structure analysis in Section 3.2, with increasing preparation time, the BET surface area of hydrochars dramatically increased. However, based on Fig. 4(c), little effect on As adsorption capacity was observed when increasing the preparation time, indicating that As adsorption was not primarily due to physical adsorption.

The iron-modified hydrochar with the highest As adsorption capacity, namely 8%FN@HC, was chosen for kinetic analysis. The characteristic adsorption time was determined by utilizing pseudo-first-order and pseudo-second-order kinetic models (Equations 1 and 2) to characterize the adsorption kinetics of As(III) and As(V).

Pseudo first-order: $q_t = Q_e\left(1\text{-}e^{-k_1 t}\right)$ (1)

Pseudo second-order: $q_t = k_2 {Q_e}^2 t/\left(1 + k_2 {Q_e}^2 t\right)$ (2)

Where Q_e was the equilibrium adsorption capacity (mg/g), t denotes the adsorption time (min), and k_1 and k_2 respectively represent the pseudo first-order and pseudo second-order adsorption rate constants.

The findings of the kinetic analysis were depicted in Fig. S4 and Table S3. The R^2 of the pseudo-second-order model was higher than that of the pseudo-first-order model. Consequently, it can be inferred that the adsorption rate was affected by the square of the number of empty sites on the adsorbent surface, and that the chemisorption mechanism governed the adsorption process(Lin et al., 2019b), which was in accordance with the conclusion that arsenic adsorption by iron-modified hydrochars occurred primarily via complexation.

To demonstrate the association between the concentrations of As(III) and As(V) in aqueous solution and the adsorption mechanism, surface properties, and affinity of the hydrochars, in this investigation, the Langmuir and Freundlich adsorption isotherms (Equations 3 and 4) were used, which are two of the most frequently used models, and Fig. S5 and Table S4 illustrate the relevant parameters.

Freundlich: $q_e(C_e) = K_F {C_e}^{\frac{1}{n}}$ (3)

Langmuir: $q_e(C_e) = q_{max} K_L C_e/\left(1 + K_L C_e\right)$ (4)

In the formula, C_e was the concentration of As( ) and As( ) at the equilibrium (mg/g), q_{max} represents the maximal equilibrium adsorption capacity (mg/g), while K_L stands for the Langmuir adsorption equilibrium constant. K_F represents the Freundlich constant for the saturable adsorption capacity of the hydrochar, while n is the correction factor. R^2 of the Freundlich model was greater than that of the Langmuir model, according to Table S4. It can be inferred that the As adsorption by 8%FN@HC includes multi-layer adsorption on the surface of the hydrochar, Fe–O functional groups and other non-uniform surfaces(Song et al., 2019). Moreover, different from Langmuir adsorption model(Dong et al., 2017; Li et al., 2016),

Freundlich adsorption model with better fitting indicated that evident non-uniformity of iron-modified hydrochars may be generated during the one-step HTC process, which may be due to the insufficient pore structure of hydrochar and the loading of Fe.

In order to evaluate the characteristics of adsorption of As(III) and As(V) by the iron-modified hydrochar in this investigation, the arsenic adsorption capacities of other materials were enumerated in Table 1. Although it was difficult to directly compare the As adsorption capacity by different materials considering their different initial concentration, adsorbent dosage, and pH, et al., the iron-modified hydrochar in this study still showed a good As adsorption capacity. In Table 1, 8%FN@HC prepared in this study has the best As adsorption capacity and its q_{max} was significantly higher than that of commercial GFH/GFO (maximum about 2.701 mg/g) adsorbents for arsenic removal from drinking water. Moreover, the iron-modified hydrochars was synthesized in one-step HTC process and its cost was relatively low. Thus, considering its high arsenic adsorption capacity, low cost and simple preparation method, the iron-modified hydrochar developed in this paper has the potential to be a promising remediation material for arsenic contamination.

Table 1. Comparison of the As(III) and As(V) adsorption capacities of various adsorption materials

Adsorbent material	valent state of Arsenic	Initial conc. (mg/L)	pH	Dosage (g/L)	q_{max} (mg/g)	Best fit isotherm model	Best fit kinetic model	Reference
Iron coated poplar hydrochar	As( )/ As( )	0.5–40	7–9	2	11.19	Freundlich	Pseudo-second order	This research
Iron coated hydrochar from olive pomace	As( )	0–20	NR	2	4.1	Langmuir	Pseudo-second order	(Capobianco et al., 2020)
Two-phase iron coated hydrochar from olive pomace	As( )	15	5	2	2.67	NR	NR	(Di Caprio et al., 2022)
Corn stem biochar impregnated with Fe-Mn Oxides	As( )/ As( )	10–50	3–7	5	8.8	Freundlich	Pseudo-second order	(Lin et al., 2019a)
Bacillus load onto Fe_3O_4 Rice straw biochar	As( )	5–20	2–9	2.5	6.08	Langmuir	Pseudo-second order	(Wang, L. et al., 2021)

3.5. As adsorption mechanism

The adsorption data of As(III) and As( ) by 8%FN@HC were well described by Freundlich and Langmuir isotherms, which showed that As(III) and As( ) covered the surfaces of the hydrochars in single and multilayers(Ahmad et al., 2018). The kinetic results showed that the pseudo-second-order model has a better fitting, indicating that the rate-limiting step was chemisorption, which may involve the interaction of surface functional groups, resulting in surface complexation(Zhang and Gao, 2013). The protons of surface functional groups may also have undergone ion exchange with them in solution. Priyadarshni reported similar results, believing that the chemical interaction between surface functional groups and metal ions was the primary mechanism controlling As(III) and As( ) adsorption(Priyadarshni et al., 2020). Moreover, based on the analysis in Section 3.4, physical adsorption based on pore structure was not the primary reason for As adsorption.

To further analyze the arsenic removal mechanism of iron-modified hydrochars, XPS characterization of both the fresh and the used 8%FN@HC was performed as shown in Fig. 5. Figure 5 (a) showed the full spectrum scan, where the As 3dd characteristic peak can be observed, indicating that As(V) was adsorbed on the surface of 8%FN@HC. Moreover, As(III) was also observed, indicating that redox process also existed in the adsorption process. Based on Fig. 5(e), C = O, –OH, Fe–O, and other oxygen groups can be observed on the surface of 8%FN@HC and –OH structures was the main group(Xu et al., 2022). After As(V) adsorption, the content of –OH and C = O decreased significantly, indicating that Fe–OH structure played a role in arsenic adsorption. Based on Fe 2p spectrum, for fresh 8%FN@HC, the content of Fe(III) was 1.24 times that of Fe(II). However, for 8%FN@HC, the ratio decreased to 0.93. Thus, it can be inferred that Fe(III) was the main component that reacts with arsenic. Moreover, it can be observed that Fe 2p spectrum of used 8%FN@HC migrated towards to higher binding energy compared to that of fresh %FN@HC, which may due to the formation of As–O–Fe structure(Lyu et al., 2022). Based on the above analysis, it can be concluded that electrostatic attraction and surface complexation are the two main mechanisms of As adsorption by iron-modified hydrochars as shown in Fig. 6. Firstly, some Fe–OH on the surface of iron-modified hydrochar was transformed to Fe–OH^{2+}, resulting in the weak protonation of –OH groups. These positively charged sites is easy to form electrostatic attraction with $H_2AsO_4^-$ or $HAsO_4^{2-}$ ions(Huang et al., 2020; Sun et al., 2022). Secondly, The –OH group in the α-Fe_2O_3 center on the surface of iron-modified hydrochar can be exchanged directly by As (ligand exchange) to form an inner arsenic complex between iron-modified hydrochar. The inner arsenic complex formation may involve monodentate binuclear-bridging mode of which the coordination occurs via As and a Fe center or/and bidentate binuclear–bridging mode of which the coordination occurs via –O– and two adjacent Fe centers.

3.6. Role of FN in HTC

Compared to FS and FC, hydrochar modified by FN in this paper was proved to have better pore structure, higher iron retention rate and higher As adsorption capacity. Therefore, it was necessary to analyze the role of FN in the HTC process. Firstly, FN dissociated into Fe^{3+} and NO_3^- in water, which significantly increased the dielectric constant of the liquid phase during the HTC process. Then, NO_3^- can form HNO_3, which can be further split into NO_2• and •OH when the reaction temperature of HTC exceeded 200°C. The mechanisms were listed as follows(Park and Lin, 2009; Shan et al., 2014):

$$HNO_3 \rightarrow NO_2\cdot + \bullet OH$$

$$NH_3 + \bullet OH \rightarrow NH_2\bullet + H_2O$$

$$NH_X + NO_2\cdot \rightarrow HNO_3 + NH_XNO \rightarrow N_2 + H_2O$$

Studies have shown that •OH promotes the formation of hydroxyl derivatives and further oxidation of carboxylic acid derivatives(Koshani et al., 2018). During HTC process, FN promoted the release of free radicals, which can break the carbon bond of biomass raw material and low molecular compounds were thus released into the liquid phase. When the reaction temperature of HTC exceeded 200°C, dehydration, decarboxylation, radical oxidation can both be enhanced during HTC process. Based on Fig.S3 and Table S2, a large number of 2-20nm pores can be observed in hydrochar modified by FN and the pore volume of 6%FN@HC was 3.6 and 10.4 times that of 6%FS@HC and 6%FC@HC, respectively. Thus, the pore structure of hydrochar modified by FN was significantly improved due to the existence of ·OH, which can provide more loading sites for iron oxide. Based on Fig. 2, a large number of iron oxide nanoparticles were loaded into the pores of hydrochar modified by FN because of their consistent size. Thus, the iron loading capacity of hydrochar modified by FN was obviously higher than that modified by FS and FC. The As adsorption capacity of hydrochar modified by FN was thus better. Based on the above analysis, it can be confirmed that by providing ·OH, FN can significantly enhance the hydrolysis process in HTC and improve the pore structure of hydrochar to further promote the loading of iron and greatly improve the As adsorption capacity.

4. Conclusions

In this study, hydrochars with stable iron loading were successfully synthesized in one-step HTC process and were used As adsorbents to remove As( ) and As( ) in aqueous phase. The Fe retention rate of hydrochars modified by FN was about 85.4%, which was significantly higher than that modified by FS and FC. This is because the iron was successfully loaded on the hydrochar when modified by FN, which can be inferred based on the characterization and ash content analysis.

The As adsorption capacity of hydrochar modified by FN was also significantly higher than those modified by FS and FC, and it increased proportionally with the increasing Fe dosage. The As adsorption mechanism was analyzed and the results showed that the surface complexation of Fe–O–As was the main reason for the adsorption of As by iron-modified hydrochar. However, physical adsorption based on pore structure played a limited role.

To analyze why the iron retention rate and As adsorption capacity of hydrochar modified by FN were significantly higher than those of hydrochars modified by FS and FC, the role of FN in HTC was studied. During HTC process, FN promoted the release of ·OH radical, which can significantly enhance the hydrolysis process and improve the pore structure of hydrochars. More iron oxide was thus loaded onto hydrochars modified by FN and its As adsorption capacity was also greatly improved. Therefore, hydrochar modified by FN was proved to be an effective material for As adsorption.

Declarations

Author Contributions Statement Authors contributions Yiwei Zhang, Conceptualization, Methodology, Formal analysis, Investigation, Resources, Data Curation, Visualization, Writing - Original Draft. Dandan Chen, Conceptualization, Methodology, Validation, Supervision, Writing - Review & Editing, Funding acquisition. Yutong Xing, Experiment, Software. Bangwei Liu, Experiment, Software. Yan Zhou, Experiment, Validation. Ping Lu, Supervision, Validation, Project administration.

Data availability The data used to support the findings of this study are available from the corresponding author upon request.

Funding The project was supported by the National Natural Science Foundation of China (52106253), the Natural Science Foundation for Young Scientists of Jiangsu Province (BK20190708), the China Postdoctoral Science Foundation (2018M642137), and the Natural Science Foundation of Universities of Jiangsu Province (18KJB470015).

Author information

Authors and Affiliations

School of Environment, Nanjing Normal University, Nanjing 210023, China;

Yiwei Zhang,

School of Energy and Mechanical Engineering, Nanjing Normal University, Nanjing 210023, China;

Yiwei Zhang, Dandan Chen, Yutong Xing, Bangwei Liu, Yan Zhou, Ping Lu

Corresponding author Correspondence to Dandan Chen

Ethical approval This study does not involve human and/or animal subjects.

Consent to participate and consent for publication All authors agreed with the content, and all gave explicit consent to submit, and they obtained consent from the responsible authorities at the institute/organization where the work has been carried out, before the work is submitted.

Declaration of Interest Statement The author(s) declared no potential conflicts of interest with respect to the research, authorship, and/or publication of this article.

References

1. Abdelrhman, F., Gao, J., Ali, U., Wan, N., Hu, H., 2022. Assessment of goethite-combined/modified biochar for cadmium and arsenic remediation in alkaline paddy soil. Environ. Sci. Pollut. Res. 29(27), 40745-40754. http://doi.org/10.1007/s11356-021-17968-4
2. Ahmad, M., Ahmad, M., Usman, A.R.A., Al-Faraj, A.S., Abduljabbar, A.S., Al-Wabel, M.I., 2018. Biochar composites with nano zerovalent iron and eggshell powder for nitrate removal from aqueous solution

with coexisting chloride ions. Environ. Sci. Pollut. Res. 25(26), 25757-25771. http://doi.org/10.1007/s11356-017-0125-9

3. Ali, S., Rizwan, M., Shakoor, M.B., Jilani, A., Anjum, R., 2020. High sorption efficiency for As(III) and As(V) from aqueous solutions using novel almond shell biochar. Chemosphere 243, 125330. https://doi.org/10.1016/j.chemosphere.2019.125330
4. Bibi, S., Farooqi, A., Yasmin, A., Kamran, M.A., Niazi, N.K., 2017. Arsenic and fluoride removal by potato peel and rice husk (PPRH) ash in aqueous environments. Int. J. Phytorem. 19(11), 1029-1036. http://dx.doi.org/10.1080/15226514.2017.1319329
5. Capobianco, L., Di Caprio, F., Altimari, P., Astolfi, M.L., Pagnanelli, F., 2020. Production of an iron-coated adsorbent for arsenic removal by hydrothermal carbonization of olive pomace: Effect of the feedwater pH. J. Environ. Manage. 273, 111164. https://doi.org/10.1016/j.jenvman.2020.111164
6. Cha, J.S., Jang, S.-H., Lam, S.S., Kim, H., Kim, Y.-M., Jeon, B.-H., Park, Y.-K., 2021. Performance of CO_2 and Fe-modified lignin char on arsenic (V) removal from water. Chemosphere 279, 130521. https://doi.org/10.1016/j.chemosphere.2021.130521
7. Chen, Q., Zhang, T.C., Ouyang, L., Yuan, S., 2022. Single-Step Hydrothermal Synthesis of Biochar from H_3PO_4-Activated Lettuce Waste for Efficient Adsorption of Cd(II) in Aqueous Solution. molecules 27(1), 269. https://doi.org/10.3390/molecules27010269
8. Chin, J.F., Heng, Z.W., Teoh, H.C., Chong, W.C., Pang, Y.L., 2022. Recent development of magnetic biochar crosslinked chitosan on heavy metal removal from wastewater-Modification, application and mechanism. Chemosphere 291,130521. http://dx.doi.org/10.1016/j.chemosphere.2021.133035
9. Cychosz, K.A., Thommes, M., 2018. Progress in the Physisorption Characterization of Nanoporous Gas Storage Materials. Engineering 4(4), 559-566. https://doi.org/10.1016/j.eng.2018.06.001
10. da Silva, E.B., Mussoline, W.A., Wilkie, A.C., Ma, L.Q., 2019. Arsenic removal and biomass reduction of As-hyperaccumulator Pteris vittata: Coupling ethanol extraction with anaerobic digestion. Sci. Total Environ. 666, 205-211. https://doi.org/10.1016/j.scitotenv.2019.02.161
11. Di Caprio, F., Pellini, A., Zanoni, R., Astolfi, M.L., Altimari, P., Pagnanelli, F., 2022. Two-phase synthesis of Fe-loaded hydrochar for As removal: The distinct effects of initial pH, reaction time and Fe/hydrochar ratio. J. Environ. Manage. 302, 114058.
12. Dong, S., Wang, Y., Zhao, Y., Zhou, X., Zheng, H., 2017. La3+/La(OH)3 loaded magnetic cationic hydrogel composites for phosphate removal: Effect of lanthanum species and mechanistic study. Water Res. 126, 433-441. https://doi.org/10.1016/j.watres.2017.09.050
13. Falco, C., Baccile, N., Titirici, M.M.J.G.C., 2011. Morphological and structural differences between glucose, cellulose and lignocellulosic biomass derived hydrothermal carbons. 13(11), 3273-3281.
14. Fang, J., Zhan, L., Ok, Y.S., Gao, B., 2018. Minireview of potential applications of hydrochar derived from hydrothermal carbonization of biomass. J. Ind. Eng. Chem. 57, 15-21. http://dx.doi.org/10.1016/j.jiec.2017.08.026
15. Gong, H.B., Zhao, L., Rui, X., Hu, J.W., Zhu, N.W., 2022. A review of pristine and modified biochar immobilizing typical heavy metals in soil: Applications and challenges. J. Hazard. Mater. 432.

http://dx.doi.org/10.1016/j.jhazmat.2022.128668

16. Gonzalez-Dominguez, J.M., Baigorri, A., Alvarez-Sanchez, M.A., Colom, E., Villacampa, B., Anson-Casaos, A., Garcia-Bordeje, E., Benito, A.M., Maser, W.K., 2021. Waterborne Graphene- and Nanocellulose-Based Inks for Functional Conductive Films and 3D Structures. Nanomaterials 11(6). http://dx.doi.org/10.3390/nano11061435
17. Hao, L.L., Liu, M.Z., Wang, N.N., Li, G.J., 2018. A critical review on arsenic removal from water using iron-based adsorbents. RSC Adv. 8(69), 39545-39560. http://dx.doi.org/10.1039/c8ra08512a
18. Huang, Y., Gao, M., Deng, Y., Khan, Z.H., Liu, X., Song, Z., Qiu, W., 2020. Efficient oxidation and adsorption of As(III) and As(V) in water using a Fenton-like reagent, (ferrihydrite)-loaded biochar. Sci. Total Environ. 715, 136957. https://doi.org/10.1016/j.scitotenv.2020.136957
19. Jain, A., Balasubramanian, R., Srinivasan, M.P., 2016. Hydrothermal conversion of biomass waste to activated carbon with high porosity: A review. Chem. Eng. J. 283, 789-805. http://dx.doi.org/10.1016/j.cej.2015.08.014
20. Khan, T.A., Saud, A.S., Jamari, S.S., Rahim, M.H.A., Park, J.-W., Kim, H.-J., 2019. Hydrothermal carbonization of lignocellulosic biomass for carbon rich material preparation: A review. Biomass Bioenergy 130, 105384. https://doi.org/10.1016/j.biombioe.2019.105384
21. Koshani, R., van de Ven, T.G.M., Madadlou, A., 2018. Characterization of Carboxylated Cellulose Nanocrystals Isolated through Catalyst-Assisted H2O2 Oxidation in a One-Step Procedure. J. Agric. Food. Chem. 66(29), 7692-7700. http://dx.doi.org/10.1021/acs.jafc.8b00080
22. Li, J., Fan, Q.H., Wu, Y.J., Wang, X.X., Chen, C.L., Tang, Z.Y., Wang, X.K., 2016. Magnetic polydopamine decorated with Mg-Al LDH nanoflakes as a novel bio-based adsorbent for simultaneous removal of potentially toxic metals and anionic dyes. J. Mater. Chem. A 4(5), 1737-1746. http://dx.doi.org/10.1039/c5ta09132b
23. Li, J., Li, L., Suvarna, M., Pan, L., Tabatabaei, M., Ok, Y.S., Wang, X., 2022. Wet wastes to bioenergy and biochar: A critical review with future perspectives. Sci. Total Environ. 817, 152921. https://doi.org/10.1016/j.scitotenv.2022.152921
24. Li, X., Zhao, C., Zhang, M., 2019. Chapter 8 - Biochar for Anionic Contaminants Removal From Water, in: Ok, Y.S., Tsang, D.C.W., Bolan, N., Novak, J.M. (Eds.), Biochar from Biomass and Waste. Elsevier, pp. 143-160. https://doi.org/10.1016/B978-0-12-811729-3.00008-X
25. Liang, J., Li, X., Yu, Z., Zeng, G., Luo, Y., Jiang, L., Yang, Z., Qian, Y., Wu, H., 2017. Amorphous MnO_2 Modified Biochar Derived from Aerobically Composted Swine Manure for Adsorption of Pb(II) and Cd(II). ACS Sustainable Chem. Eng. 5(6), 5049-5058. http://dx.doi.org/10.1021/acssuschemeng.7b00434
26. Liang, L., Xi, F., Tan, W., Meng, X., Hu, B., Wang, X., 2021. Review of organic and inorganic pollutants removal by biochar and biochar-based composites. Biochar 3(3), 255-281. http://dx.doi.org/10.1007/s42773-021-00101-6
27. Lin, L., Song, Z., Huang, Y., Khan, Z.H., Qiu, W., 2019a. Removal and Oxidation of Arsenic from Aqueous Solution by Biochar Impregnated with Fe-Mn Oxides. Water Air Soil Pollut. 230(5), 105. http://dx.doi.org/10.1007/s11270-019-4146-5

28. Lin, L., Song, Z., Khan, Z.H., Liu, X., Qiu, W., 2019b. Enhanced As(III) removal from aqueous solution by Fe-Mn-La-impregnated biochar composites. Sci. Total Environ. 686, 1185-1193. https://doi.org/10.1016/j.scitotenv.2019.05.480
29. Liu, M., Sun, F., Lv, Y., Xu, Y., Li, M., Wang, Y., Yin, X., Jiang, H., 2021. Remediation of arsenic-contaminated soil by nano-zirconia modified biochar. Environ. Sci. Pollut. Res. 28(48), 68792-68803. http://dx.doi.org/10.1007/s11356-021-15362-8
30. Liu, Z., Wang, Z., Chen, H., Cai, T., Liu, Z., 2021. Hydrochar and pyrochar for sorption of pollutants in wastewater and exhaust gas: A critical review. Environ. Pollut. 268, 115910. https://doi.org/10.1016/j.envpol.2020.115910
31. Luo, X., Huang, Z., Lin, J., Li, X., Qiu, J., Liu, J., Mao, X., 2020. Hydrothermal carbonization of sewage sludge and in-situ preparation of hydrochar/MgAl-layered double hydroxides composites for adsorption of Pb(II). J. Cleaner Prod. 258, 120991. https://doi.org/10.1016/j.jclepro.2020.120991
32. Lyu, H., Tang, J., Cui, M., Gao, B., Shen, B., 2020. Biochar/iron (BC/Fe) composites for soil and groundwater remediation: Synthesis, applications, and mechanisms. Chemosphere 246, 125609. https://doi.org/10.1016/j.chemosphere.2019.125609
33. Lyu, P., Li, L., Huang, X., Wang, G., Zhu, C., 2022. Pre-magnetic bamboo biochar cross-linked CaMgAl layered double-hydroxide composite: High-efficiency removal of As(III) and Cd(II) from aqueous solutions and insight into the mechanism of simultaneous purification. Sci. Total Environ. 823, 153743. https://doi.org/10.1016/j.scitotenv.2022.153743
34. Ma, X.-Q., Shan, Y.-Q., Duan, P.-G., Liao, J.-J., Chen, D.-B., Xu, Z.-X., 2021. $Fe(NO_3)_3$ assisted hydrothermal carbonization of sewage sludge: Focusing on characteristics of hydrochar and aqueous phase. Mol. Catal. 514, 111823. https://doi.org/10.1016/j.mcat.2021.111823
35. Medunić, G., Fiket, Ž., Ivanić, M., 2020. Arsenic Contamination Status in Europe, Australia, and Other Parts of the World, in: Srivastava, S. (Ed.) Arsenic in Drinking Water and Food. Springer Singapore, Singapore, pp. 183-233.
36. Oliveira, R.C., Hammer, P., Guibal, E., Taulemesse, J.-M., Garcia, O., 2014. Characterization of metal–biomass interactions in the lanthanum(III) biosorption on Sargassum sp. using SEM/EDX, FTIR, and XPS: Preliminary studies. Chem. Eng. J. 239, 381-391. https://doi.org/10.1016/j.cej.2013.11.042
37. Park, J., Lin, M.C., 2009. Thermal Decomposition of Gaseous Ammonium Nitrate at Low Pressure: Kinetic Modeling of Product Formation and Heterogeneous Decomposition of Nitric Acid. J. Phys. Chem. A 113(48), 13556-13561. http://dx.doi.org/10.1021/jp9058005
38. Priyadarshni, N., Nath, P., Nagahanumaiah, Chanda, N., 2020. Sustainable removal of arsenate, arsenite and bacterial contamination from water using biochar stabilized iron and copper oxide nanoparticles and associated mechanism of the remediation process. J. Water Process Eng. 37, 101495. https://doi.org/10.1016/j.jwpe.2020.101495
39. Rashid, R., Shafiq, I., Akhter, P., Iqbal, M.J., Hussain, M., 2021. A state-of-the-art review on wastewater treatment techniques: the effectiveness of adsorption method. Environ. Sci. Pollut. Res. 28(8), 9050-9066. http://dx.doi.org/10.1007/s11356-021-12395-x

40. Shan, T.-R., van Duin, A.C.T., Thompson, A.P., 2014. Development of a ReaxFF Reactive Force Field for Ammonium Nitrate and Application to Shock Compression and Thermal Decomposition. The Journal of Physical Chemistry A 118(8), 1469-1478. http://dx.doi.org/10.1021/jp408397n
41. Song, X.L., Zhou, L., Zhang, Y., Chen, P., Yang, Z.L., 2019. A novel cactus-like Fe_3O_4/Halloysite nanocomposite for arsenite and arsenate removal from water. J. Cleaner Prod. 224, 573-582. http://dx.doi.org/10.1016/j.jclepro.2019.03.230
42. Sorlini, S., Gialdini, F., Collivignarelli, M.C., 2014. Survey on full-scale drinking water treatment plants for arsenic removal in Italy. Water Practice and Technology 9(1), 42-51. http://dx.doi.org/10.2166/wpt.2014.005
43. Sun, Y.C., Yu, F.X., Han, C.H., Houda, C., Hao, M.G., Wang, Q.Y., 2022. Research Progress on Adsorption of Arsenic from Water by Modified Biochar and Its Mechanism: A Review. Water 14(11). http://dx.doi.org/10.3390/w14111691
44. Thommes, M., Kaneko, K., Neimark, A.V., Olivier, J.P., Rodriguez-Reinoso, F., Rouquerol, J., Sing, K.S.W., 2015. Physisorption of gases, with special reference to the evaluation of surface area and pore size distribution (IUPAC Technical Report). Pure Appl. Chem. 87(9-10), 1051-1069. http://dx.doi.org/10.1515/pac-2014-1117
45. Vieira, B.R.C., Pintor, A.M.A., Boaventura, R.A.R., Botelho, C.M.S., Santos, S.C.R., 2017. Arsenic removal from water using iron-coated seaweeds. J. Environ. Manage. 192, 224-233. https://doi.org/10.1016/j.jenvman.2017.01.054
46. Wan, X., Li, C., Parikh, S.J., 2020. Simultaneous removal of arsenic, cadmium, and lead from soil by iron-modified magnetic biochar. Environ. Pollut. 261, 114157. https://doi.org/10.1016/j.envpol.2020.114157
47. Wang, H., Xu, J., Liu, X., Sheng, L., 2021. Preparation of straw activated carbon and its application in wastewater treatment: A review. J. Cleaner Prod. 283, 124671. https://doi.org/10.1016/j.jclepro.2020.124671
48. Wang, L., Li, Z., Wang, Y., Brookes, P.C., Wang, F., Zhang, Q., Xu, J., Liu, X., 2021. Performance and mechanisms for remediation of Cd(II) and As(III) co-contamination by magnetic biochar-microbe biochemical composite: Competition and synergy effects. Sci. Total Environ. 750, 141672. https://doi.org/10.1016/j.scitotenv.2020.141672
49. Xu, Z., Wan, Z., Sun, Y., Gao, B., Hou, D., Cao, X., Komárek, M., Ok, Y.S., Tsang, D.C.W., 2022. Electroactive Fe-biochar for redox-related remediation of arsenic and chromium: Distinct redox nature with varying iron/carbon speciation. J. Hazard. Mater. 430, 128479. https://doi.org/10.1016/j.jhazmat.2022.128479
50. Zhang, F., Wang, X., Xionghui, J., Ma, L., 2016. Efficient arsenate removal by magnetite-modified water hyacinth biochar. Environ. Pollut. 216, 575-583. https://doi.org/10.1016/j.envpol.2016.06.013
51. Zhang, M., Gao, B., 2013. Removal of arsenic, methylene blue, and phosphate by biochar/AlOOH nanocomposite. Chem. Eng. J. 226, 286-292. https://doi.org/10.1016/j.cej.2013.04.077
52. Zhang, Y., Lu, P., Chen, D., Song, T., 2021. Effect of operation conditions on fuel characteristics of hydrochar via hydrothermal carbonization of agroforestry biomass. Biomass Convers. Biorefin.

http://dx.doi.org/10.1007/s13399-021-02003-w

53. Zhu, S., Zhao, J., Zhao, N., Yang, X., Chen, C., Shang, J., 2020. Goethite modified biochar as a multifunctional amendment for cationic Cd(II), anionic As(III), roxarsone, and phosphorus in soil and water. J. Cleaner Prod. 247, 119579. /https://doi.org/10.1016/j.jclepro.2019.119579
54. Zoroufchi Benis, K., Motalebi Damuchali, A., Soltan, J., McPhedran, K.N., 2020. Treatment of aqueous arsenic – A review of biochar modification methods. Sci. Total Environ. 739, 139750. https://doi.org/10.1016/j.scitotenv.2020.139750

Figures

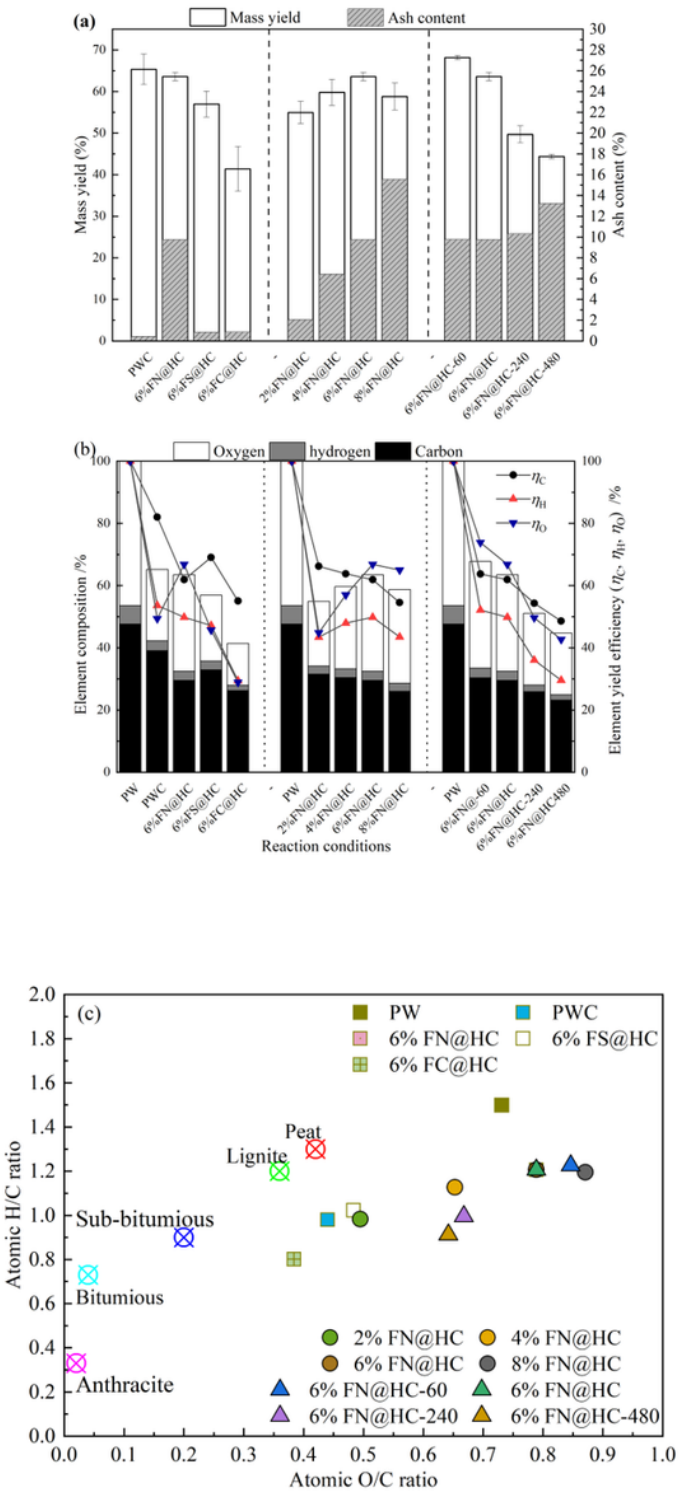

Figure 1

Effects of iron species, iron dosage, and preparation time on (a) mass yield and ash content, (b) element composition and element yield efficiency of iron-modified hydrochars and (c) Van Krevelen diagram of unmodified and iron-modified hydrochars

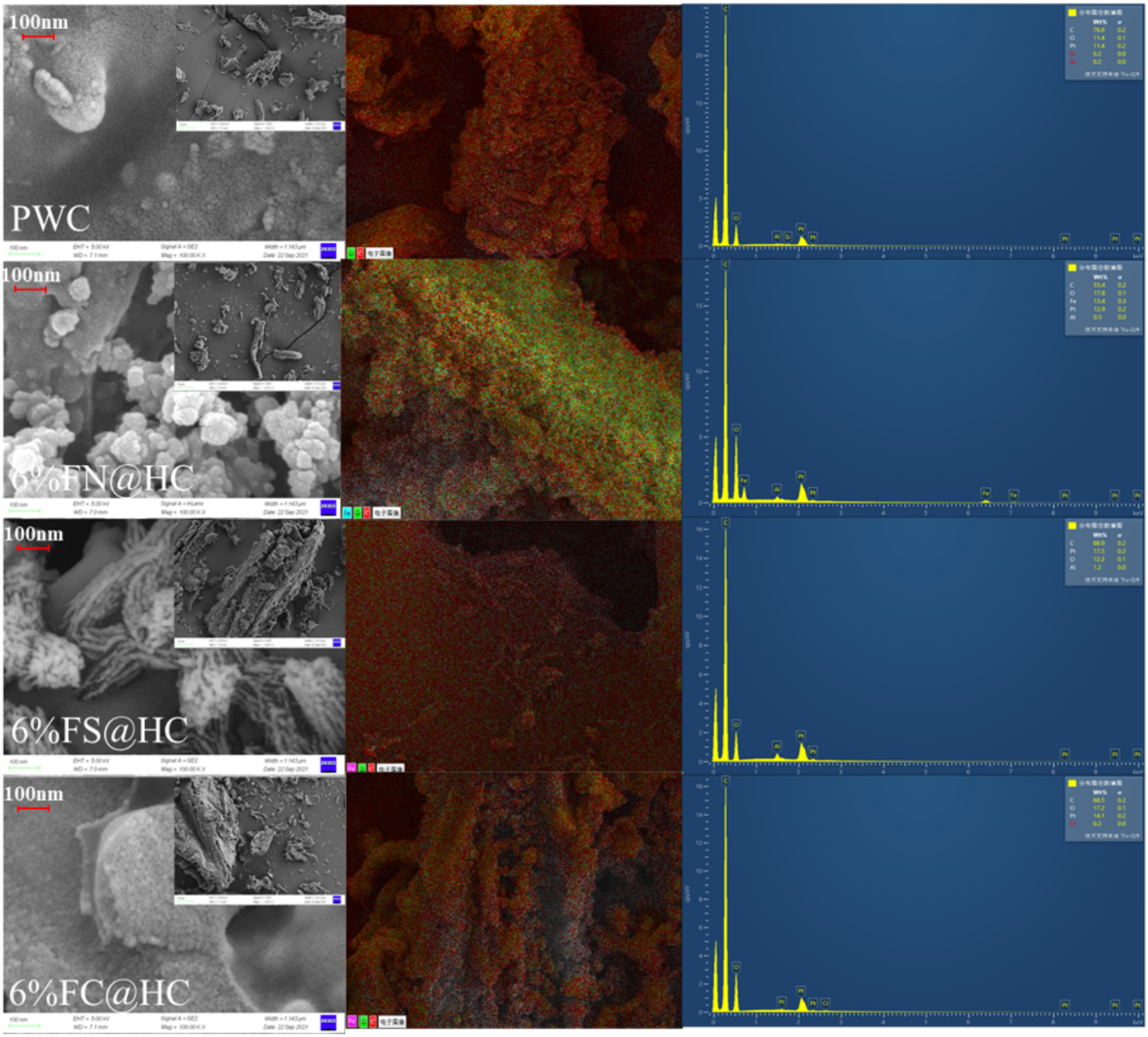

Figure 2

SEM and SEM-MAPPING of hydrochars modified by different iron species

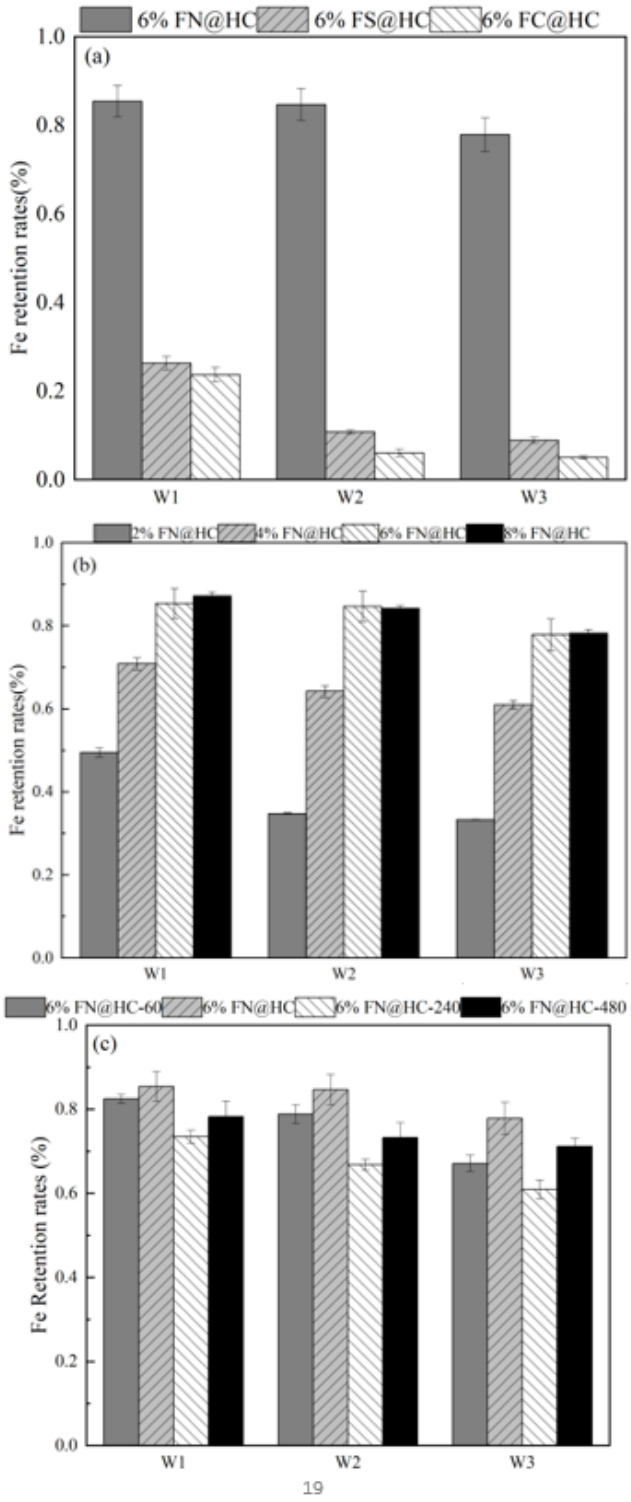

Figure 3

Iron retention rate of the iron-modified hydrochars (relative to the total amount added in liquid phase %)

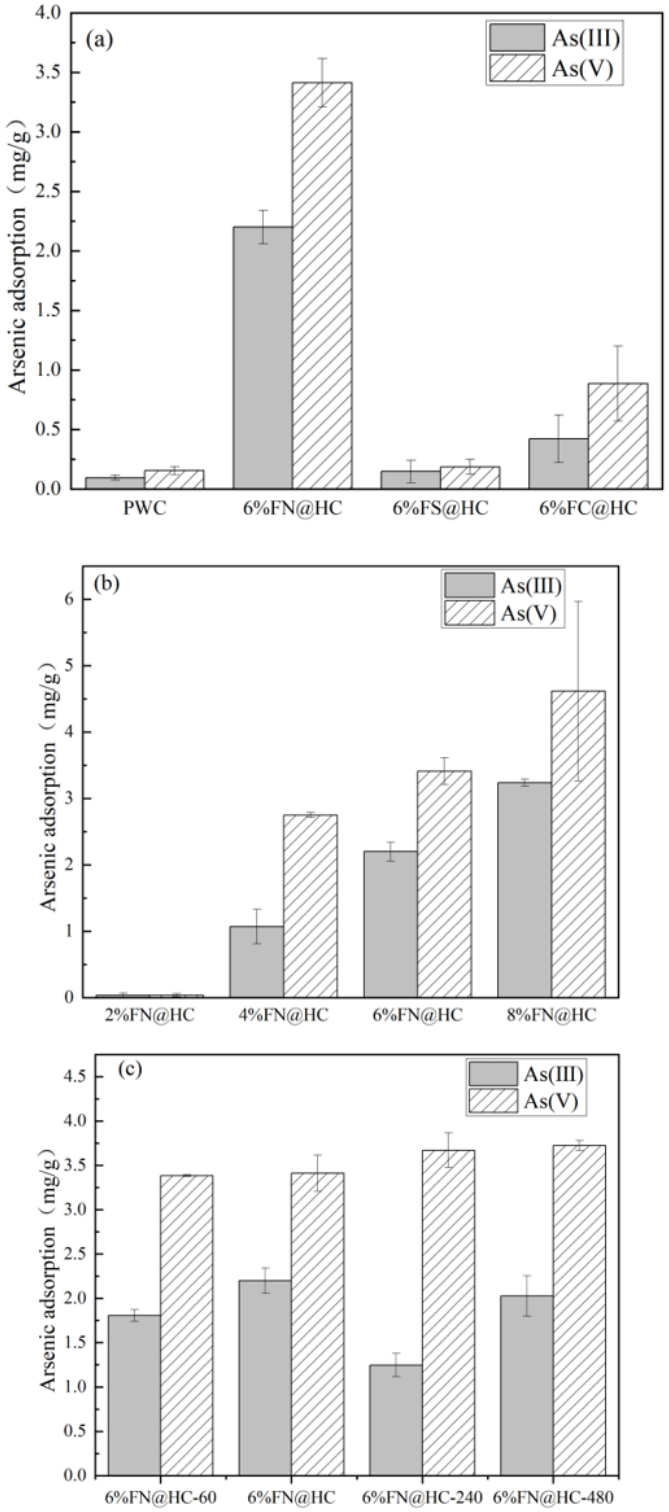

Figure 4

As adsorption characteristics of hydrochars modified under different conditions: (a) different iron species, (b) different iron dosage, and (c) different preparation time

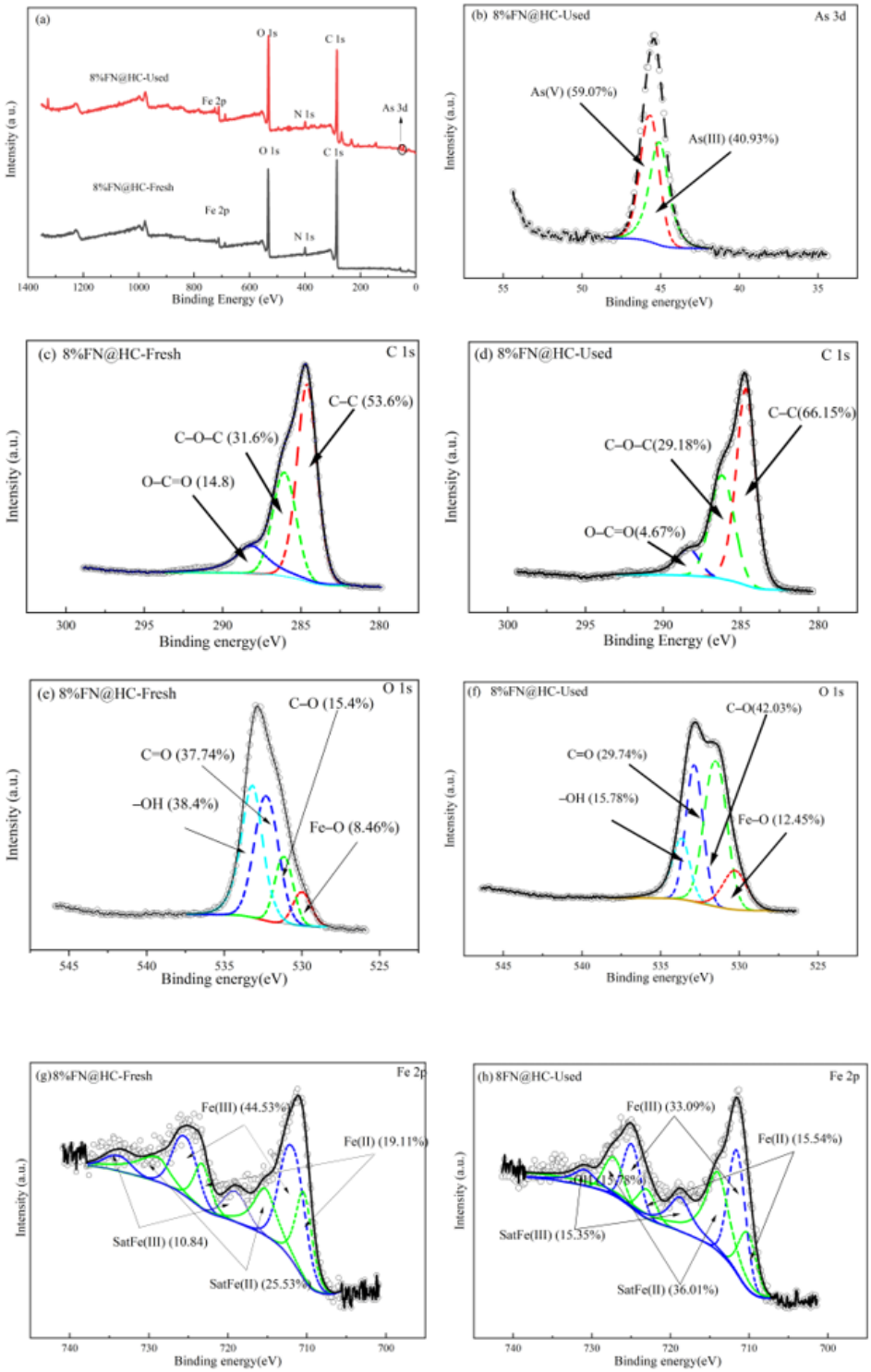

Figure 5

XPS spectra of fresh and used iron-modified hydrochar. (a) wide scan (b) As 3d spectrum (c), (d) C1s spectrum (e), (f) O 1s spectrum (g), (h) Fe 2p spectrum

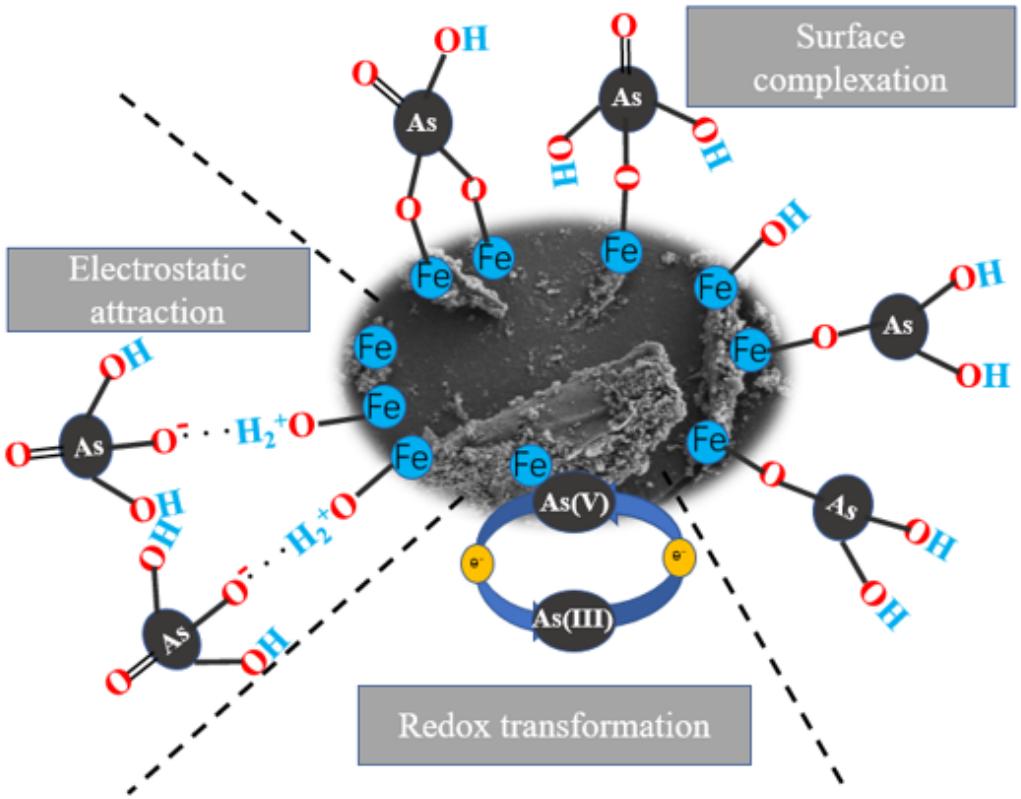

Figure 6

The As adsorption mechanism on the surface of iron-modified hydrochar

Supplementary Files

This is a list of supplementary files associated with this preprint. Click to download.

- GraphicalAbstract.png
- SupplementaryMaterial.docx